Journal of Alloys and Compounds 513 (2012) 436–444

Contents lists available at SciVerse ScienceDirect

Journal of Alloys and Compounds

journal homepage: www.elsevier.com/locate/jallcom

Rietveld refinement, electrical properties and magnetic characteristics of Ca–Sr substituted barium hexaferrites

Ashima, Sujata Sanghi, Ashish Agarwal*, Reetu

Department of Applied Physics, Guru Jambheshwar University of Science & Technology, Hisar 125001, Haryana, India

ARTICLE INFO

Article history:
Received 28 June 2011
Received in revised form 18 October 2011
Accepted 19 October 2011
Available online 7 November 2011

Keywords:
Hexaferrite
Rietveld refinement
Dielectric properties
Magnetic properties

ABSTRACT

M-type Ca–Sr substituted barium hexaferrites having compositions $BaFe_{12}O_{19}$, $Ba_{0.5}Ca_{0.5}Fe_{12}O_{19}$ and $Ba_{0.5}Ca_{0.25}Sr_{0.25}Fe_{12}O_{19}$ have been synthesized by commercial solid state reaction method. The effects of doping on structural, dielectric and magnetic properties were systematically investigated. The Rietveld refinement of X-ray powder diffraction data revealed that the samples possess single hexagonal phase with space group $P6_3/mmc$, with two molecules in the unit cell (Z = 2). However, in $Ba_{0.5}Ca_{0.5}Fe_{12}O_{19}$ sample, a secondary phase (Fe_2O_3) is also present with space group R3c with six molecules in the unit cell (Z = 6). SEM results show a heterogeneous distribution of grain sizes within the samples. The dc electrical resistivity (ρ) has been measured as a function of temperature. The variation of dielectric constant (ε') and dielectric loss ($\tan\delta$) with temperature and frequency were analyzed on the basis of Maxwell–Wagner and Koops' models. Lower saturation magnetization and increased coercivity is observed in substituted samples.

© 2011 Elsevier B.V. All rights reserved.

1. Introduction

Excessive demand for M-type hexaferrites, due to their exclusively high electrical resistivity and low eddy current losses, has initiated exhaustive research efforts to synthesize these for use as stable permanent magnets with best performance-to-cost ratio [1]. Hexaferrites are classified into five types depending on chemical and crystalline structure. These are M, W, Y, X and Z type hexaferrites corresponding to (BaO + MeO):Fe_2O_3 ratio (where Me is transition metal) of 1:6, 3:8, 4:6, 4:14 and 5:12, respectively [2]. The M type hexaferrites crystallize in a hexagonal structure with 64 ions per unit cell on 11 different symmetry sites. The 24 Fe^{3+} ions are distributed over five different sites: three octahedral (B) sites (12k, 2a, $4f_2$), one tetrahedral (A) site ($4f_1$) and one trigonal bipyramidal (C) site (2b), which is not found with spinel structures [3]. The hexagonal ferrites, $MFe_{12}O_{19}$ (M = Ba, Sr, Pb) with the magnetoplumbite structure continue to be important permanent magnetic materials in microwaves and more recently in magnetic recording applications. Such materials are known as hard ferrites due to their high values of electrical resistivity, saturation magnetization, coercivity, Curie temperature, mechanical hardness and chemical inertness. At higher frequency, hexaferrites are considered to be superior to other magnetic materials because they have low–eddy current loss and high resistivity [4]. Therefore, hexaferrites which are magnetic semiconductors have opened a new vista in physics of materials.

In the spinel structure, only 1/8 of tetrahedral holes are occupied. In magnetoplumbite, there are only 4 holes of f_{IV} and 4 holes of f_{VI} type in a unit cell and all of them are occupied by Fe^{3+} ions. Half of the 12k holes are occupied by Fe^{3+} ions for a molecule with formula $BaFe_{12}O_{19}$. Different substituting cations have been reported to preferentially occupy specific sites when doping barium hexaferrites. If the Fe^{3+} ions in different holes are selectively substituted by other cations, the magnetic properties can be altered [5]. Hexagonal ferrites have a cut-off frequency at GHz, about an order of magnitude higher than that of spinel ferrites [6]. $BaFe_{12}O_{19}$ is a well-known permanent magnet with great technical importance and have attracted an extensive attention for the last few decades. It was widely used in the fabrication of permanent magnets, computer data storage, magneto-optic recording etc. [7].

The typical method to obtain ferrimagnetic hexagonal oxide particles, in general, is the solid state reaction. In order to reduce the particle size, other methods have also been investigated such as aerosol pyrolysis, sol–gel, chemical co-precipitation, dehydration and rotary evaporation method etc. [8]. However, these methods are more complex and expensive than the ceramic method [9]. Various properties of Ba hexaferrites have been studied in the past by several groups by replacing its Fe^{3+} ions and Ba^{2+} ions with Sm^{3+}, Mn^{3+}, Ni^{2+}, Al^{3+} ions etc. and with various bivalent-tetravalent cation combinations such as Sn–Zn, Zr–Ni, Zn–Ti [10–13]. Most of the researchers worked on Ba or Sr hexaferrites and Sr-doped Ba hexaferrites. Ca also belongs to the same group in the periodic table

* Corresponding author. Tel.: +91 1662 263384; fax: +91 1662 276240.
E-mail address: aagju@yahoo.com (A. Agarwal).

0925-8388/$ – see front matter © 2011 Elsevier B.V. All rights reserved.
doi:10.1016/j.jallcom.2011.10.071

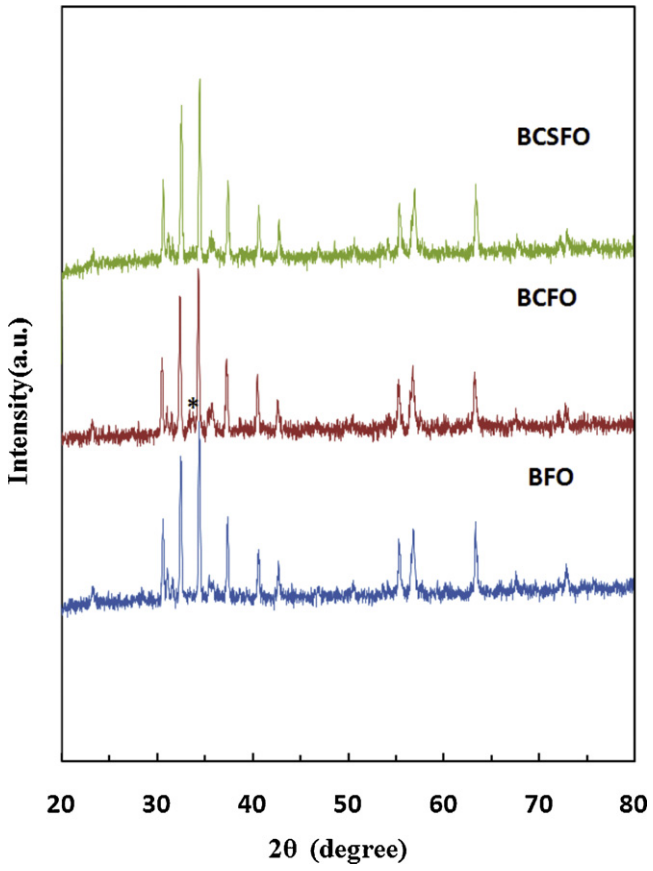

Fig. 1. X-ray diffraction patterns of prepared hexaferrites. Asterisk (*) corresponds to α-Fe_2O_3 phase.

and has same electronic configuration as that of Sr and Ba. Therefore, the synthesis of Ca, Ca–Sr doped Ba hexaferrites and effect of substitution on different dielectric and magnetic parameters are the focus of the present study.

2. Experimental details

$BaFe_{12}O_{19}$ (BFO), $Ba_{0.5}Ca_{0.5}Fe_{12}O_{19}$ (BCFO) and $Ba_{0.5}Ca_{0.25}Sr_{0.25}Fe_{12}O_{19}$ (BCSFO) samples were prepared by commercial solid state reaction method. The starting materials used were of analytical grade $BaCO_3$, $CaCO_3$, $SrCO_3$ and Fe_2O_3 of high purity. The reagents were weighed according to their stoichiometric amount and the mixed oxides were ground using an agate mortar and pestle. Then a presintering process was carried out in a furnace at 873 K for 4 h at a ramp of 5 K/min for all the powders. The powders were slowly cooled to room temperature. The grinding process was repeated again and the powders were finally sintered in the furnace at 1373 K for 4 h and were naturally cooled to room temperature. The structural properties of samples were investigated by recording their X-ray diffractograms. The X-ray diffraction patterns were obtained using a Rigaku Miniflex-II X-ray diffractometer, using Cu-Kα radiation. The ferrite powders were scanned in the range 20–80° with a scanning rate of 2°/min. The structural parameters were refined by GSAS and EXPGUI programs. The surface morphology and microstructure of samples were examined with a scanning electron microscope (JEOL JSM 6510). The dielectric properties were measured in the frequency range 1 kHz–5 MHz and temperature range 323–573 K using an impedance/gain-phase analyzer (Newton's 4th Ltd.). The samples were used in the form of pellets of about 13 mm diameter. The pellets were made at a pressure of 10 tons at room temperature. The two surfaces of sample pellets were coated with silver paste as a contact material. The dielectric constant was calculated using the formula:

$$\varepsilon' = \frac{Z''}{2\pi f C_0 \left[(Z')^2 + (Z'')^2\right]} \quad (1)$$

where f is frequency, C_0 is capacitance, Z' and Z'' are real and imaginary impedances. The resistivity ρ is calculated by the following relation:

$$\rho = R\left(\frac{A}{t}\right) \quad (2)$$

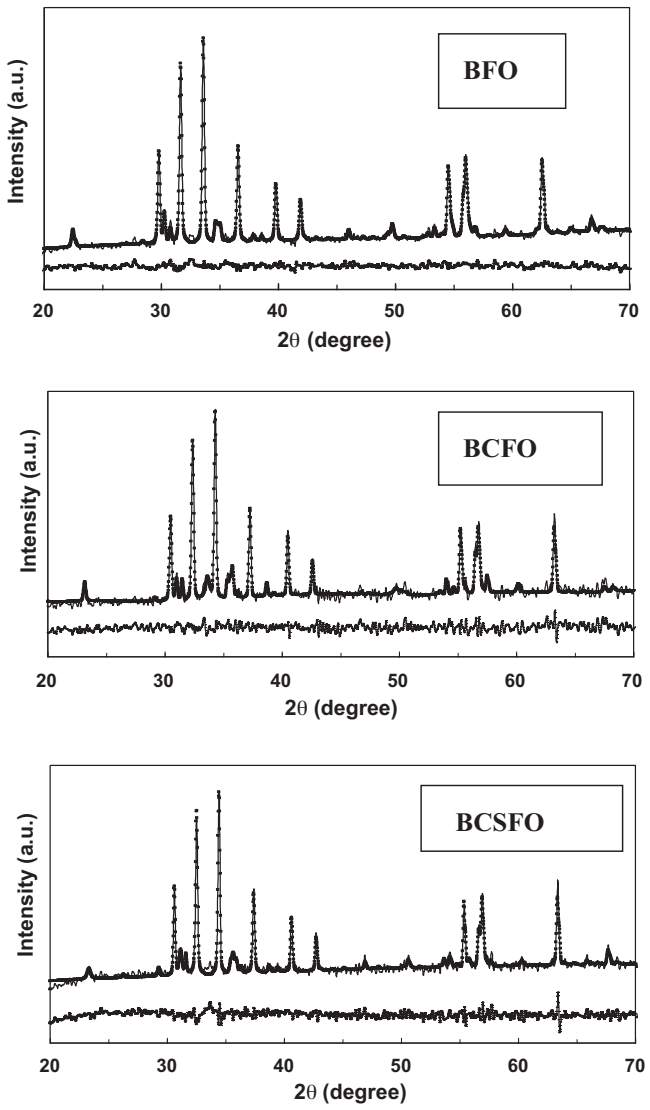

Fig. 2. Rietveld refinement data of prepared hexaferrites. The square sign shows calculated data and the continuous line overlapping them refers to raw experimental data. The difference between the experimental data and calculated data is shown at the bottom.

where R is the resistance of sample measured with the help of impedance Nyquist plots, A is area and t is thickness of pellet. The magnetic properties were measured by using vibrating sample magnetometer (Lakeshore VSM 7410) at room temperature with a maximum applied field of 20 kOe.

3. Results and discussion

3.1. XRD analysis

The X-ray diffraction patterns of all prepared hexaferrites are shown in Fig. 1. The diffractions peaks observed in the samples were identified by JCPDS file number 00-043-0002 [14]. The X-ray diffraction corresponding to BFO and BCSFO samples showed that only one phase is present, however, in BCFO sample an additional secondary phase (α-Fe_2O_3) can be seen at 33.70° (2θ). The diffraction line characteristic of α-Fe_2O_3 is identified by JCPDS file number 00-072-6227. The peak at 33.11° (2θ) characteristic of α-Fe_2O_3 has been reported in literature [2] for Ba(Sr)$Fe_{12}O_{19}$ hexaferrites prepared by ceramic method. Also the peak corresponding to α-Fe_2O_3 impurity phase was observed at 38.74° in $SrFe_{12}O_{19}$ hexaferrites prepared with sol–gel and sonochemical methods [15,16].

3.2. Rietveld analysis

The Rietveld refinement data of all the prepared hexaferrites are shown in Fig. 2. The parameters R_p (profile fitting R-value), R_{wp} (weighted profile R-value) and χ^2 (goodness-of-fit quality factor) [17] obtained after refinement (Fig. 2) are presented in Table 1. For an excellent fit, the value of χ^2 should be nearly one. For prepared samples, the value of χ^2 is less than six. Hence, the good fitting parameters suggest that the studied samples are of better quality and refinements of samples are effective. The GSAS and EXPGUI programs [18] have been used for the refinement analysis. In refinement analysis, the refined parameters were background parameters, isotropic thermal parameters, lattice parameters, scale factor, profile half-width parameters (u,v,w), occupancy and atomic functional positions. The refined structural parameters are also given in Table 1. The refined atomic positions for all the prepared hexaferrites are presented in Tables 2–4. The important bond lengths (Å) and bond angles (°) calculated for all the prepared hexaferrites are listed in Tables 5–7.

The BFO and BCSFO samples possess a hexagonal structure with space group $P6_3/mmc$ (194), with two molecules in the unit cell (Z = 2). In BCFO sample, a secondary phase is also present with space group R3c, with six molecules in the unit cell (Z = 6). The weight percent of secondary phase is nearly 3.2%. With substitutions, the value of '*a*' almost remains same but the value of '*c*' decreases due to smaller ionic radii of Ca^{2+} (0.99 Å) and Sr^{2+} (1.32 Å) as compared to Ba^{2+} (1.49 Å). Hence crystal structure becomes more compact with substitutions. Similar type of variation in cell parameters on substitutions has also been reported [1,4]. The calculated values of density also decreased with substitutions due to low values of molar mass of Ca and Sr as compared to Ba (Table 1).

3.3. Scanning electron microscopy

The SEM records of all the samples are shown in Fig. 3. The micrographs present a heterogeneous distribution of grain sizes. The grains appear to stick to each other. Some grains agglomerate in different masses. The crystallite sizes of the samples calculated by Scherrer formula are found to be in the range from 22 to 29 nm. The values of particle sizes calculated from SEM records for BFO, BCFO and BCSFO samples are 25, 22 and 29 nm, respectively. These values are in good agreement with the crystallite size of the samples calculated by using Scherrer formula. The particle sizes for the samples synthesized in the present study are much smaller as compared to those reported earlier for M-type hexaferrite [3,19]. These particle sizes are small enough to obtain the suitable signal-to-noise ratio in the high density recording media. Therefore, the synthesized samples can be used as potential material for application in recording media.

3.4. Transmission electron microscopy

Some of the micrographs of the prepared samples obtained from TEM at different magnifications are shown in Fig. 4. Closer magnification clearly shows the particle having hexagonal shape. The expected size for particles of BFO, BCFO and BCSFO hexaferrites range from 6–9, 4–6 and 10–13 nm, respectively. These particle sizes are small as compared to that obtained from XRD and SEM analysis. Similar results have also been reported by other authors [20].

3.5. Electrical properties

The electrical properties of ferrites depend upon chemical composition, method of preparation, sintering temperature and grain

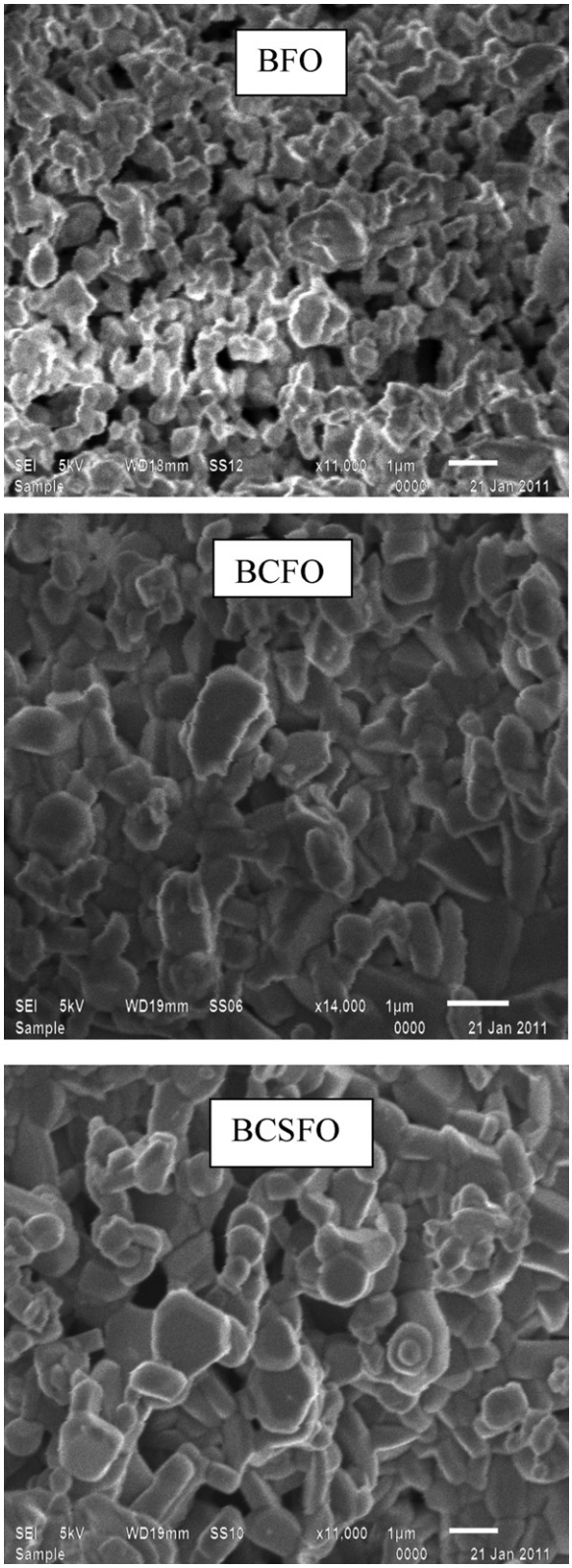

Fig. 3. SEM records of prepared hexaferrites: (a) BFO, (b) BCFO and (c) BCSFO samples.

Table 1
Refined structural parameters of prepared samples.

Sample	Space group	R_p (%)	R_{wp} (%)	χ^2	a (Å)	c (Å)	V (Å^3)	ρ (g/cm^3)	Wt. (%)
BFO	$P6_3/mmc$	0.84	1.08	1.75	5.90	23.23	699.77	5.44	100
BCFO									
First phase	$P6_3/mmc$	1.40	1.61	4.24	5.90	23.20	698.48	5.21	96.72
Second phase (Fe_2O_3)	R3c				5.06	13.55	300.51		3.28
BCSFO	$P6_3/mmc$	2.01	2.71	5.53	5.89	23.17	696.22	5.02	100

Table 2
Atomic positions obtained from Rietveld refinement for BFO sample.

Atom	Site	x	y	z
Ba	2d	0.6667	0.3333	0.2500
Fe1	2a	0.0000	0.0000	0.0000
Fe2	2b	0.0000	0.0000	0.2500
Fe3	4f1	0.3333	0.6667	0.0271
Fe4	4f2	0.3333	0.6667	0.1903
Fe5	12k	0.1713	0.3426	−0.1084
O1	4e	0.0000	0.0000	0.1450
O2	4f	0.3300	0.6667	−0.0545
O3	6h	0.1864	0.3729	0.2500
O4	12k	0.1583	0.3166	0.0514
O5	12k	0.5223	0.0447	0.1542

Table 3
Atomic positions obtained from Rietveld refinement for BCFO sample.

Atom	Site	x	y	z
Ba/Ca	2d	0.6667	0.3333	0.2500
Fe1	2a	0.0000	0.0000	0.0000
Fe2	2b	0.0000	0.0000	0.2500
Fe3	4f1	0.3333	0.6667	0.0328
Fe4	4f2	0.3333	0.6667	0.1945
Fe5	12k	0.1671	0.3341	−0.1121
O1	4e	0.0000	0.0000	0.1488
O2	4f	0.3300	0.6667	−0.0766
O3	6h	0.1518	0.3037	0.2500
O4	12k	0.1727	0.3452	0.0552
O5	12k	0.4856	−0.0280	0.1617

Table 4
Atomic positions obtained from Rietveld refinement for BCSFO sample.

Atom	Site	x	y	z
Ba/Ca/Sr	2d	0.6667	0.3333	0.2500
Fe1	2a	0.0000	0.0000	0.0000
Fe2	2b	0.0000	0.0000	0.2500
Fe3	4f1	0.3333	0.6667	0.0260
Fe4	4f2	0.3333	0.6667	0.1909
Fe5	12k	0.1685	0.3371	−0.1094
O1	4e	0.0000	0.0000	0.1549
O2	4f	0.3300	0.6667	−0.0504
O3	6h	0.1853	0.3708	0.2500
O4	12k	0.1626	0.3251	0.0548
O5	12k	0.5154	0.0309	0.1483

Table 5
Bond lengths, bond angles from Rietveld refinement for BFO sample.

Type	Bond length (Å)	Type	Bond length (Å)	Type	Bond angle (deg)
Ba-O	2.9555	Fe4-O3	2.0433	Fe5-O1-Fe5	102.351
Ba-Fe2	3.4049	Fe4-O5	2.1041	Fe3-O2-Fe5	127.163
Ba-Fe5	3.6808	Fe5-O1	1.9452	Fe2-O3-Fe4	137.247
Fe1-O4	2.0110	Fe5-O2	2.0767	Fe4-O3-Fe4	85.506
Fe2-O1	2.4382	Fe5-O4	2.1458	Fe5-O4-Fe5	89.850
Fe2-O3	1.9045	Fe5-O5	1.8984		
Fe3-O2	1.8959	Fe4-Fe4	2.7742		
Fe3-O4	1.8748	Fe5-Fe5	2.8662		

Table 6
Bond lengths, bond angles from Rietveld refinement for BCFO sample.

Type	Bond length (Å)	Type	Bond length (Å)	Type	Bond angle (°)
Ba-O	2.9518	Fe4-O3	2.2566	Fe5-O1-Fe5	101.607
Ba-Fe2	3.4041	Fe4-O5	1.7309	Fe4-O5-Fe5	131.525
Ba-Fe5	3.6219	Fe5-O1	1.9452	Fe5-O2-Fe5	102.354
Fe1-O4	2.1793	Fe5-O2	1.8874		
Fe2-O1	2.3482	Fe5-O4	2.1803		
Fe2-O3	1.5509	Fe5-O5	2.1181		
Fe3-O2	2.5369	Fe4-Fe4	2.5750		
Fe3-O4	1.7221	Fe5-Fe5	2.7665		

Table 7
Bond lengths, bond angles from Rietveld refinement for BCSFO sample.

Type	Bond length (Å)	Type	Bond length (Å)	Type	Bond angle (°)
Ba-O	2.8161	Fe4-O3	2.0337	Fe5-O1-Fe5	89.834
Ba-Fe2	3.4025	Fe4-O5	2.1051	Fe4-O3-Fe4	84.370
Ba-Fe5	3.6673	Fe5-O1	2.0181	Fe5-O4-Fe5	89.834
Fe1-O4	2.0909	Fe5-O2	2.1666	Fe2-O3-Fe4	137.815
Fe2-O1	2.2040	Fe5-O4	2.1101		
Fe2-O3	1.8926	Fe5-O5	1.8522		
Fe3-O2	1.7722	Fe4-Fe4	2.7369		
Fe3-O4	1.8667	Fe5-Fe5	2.9129		

size, etc. DC electrical resistivity as a function of temperature may be written as [21]:

$$\rho = \rho_0 \ \exp\left(\frac{E_a}{k_B T}\right) \tag{3}$$

where ρ is the dc electrical resistivity at temperature T, ρ_0 is resistivity at initial value of temperature, E_a is the activation energy and k_B is the Boltzmann's constant.

The observed decrease in dc electrical resistivity with increase in temperature (Fig. 5) is a typical behavior of semiconductors [22]. The conduction in ferrites at room temperature is due to impurities, whereas at high temperature it is due to polaron hopping. The conductivity in ferrites may be explained by Verwey's hopping mechanism [23]. According to Verwey, the electronic conduction in ferrite is mainly due to hopping of electrons between ions of the same element present in more than one valence state, distributed randomly over crystallographically different lattice sites. Hexaferrites structurally form hexagonal closed packed stacking of oxygen with cations at octahedral, trigonalbipyramidal and tetrahedral sites. The distance between two metal ions at octahedral sites is less than the distance between two metal ions at octahedral and tetrahedral sites. Therefore hopping between tetrahedral and octahedral sites has very small probability compared with that for octahedral–octahedral hopping. The hopping between tetrahedral–tetrahedral sites does not exist, due to the fact that there are only Fe^{3+} ions at tetrahedral sites and any Fe^{2+} ions formed during sintering process preferentially occupy only octahedral sites. The conduction mechanism in hexaferrites can be explained on the basis of hopping of electrons between $Fe^{3+} \leftrightarrow Fe^{2+}$ at octahedral sites, i.e.

$$Fe^{3+} + e^- \rightarrow Fe^{2+} \tag{4}$$

$$O^{2+} + 2e^- \rightarrow O \tag{5}$$

On incorporating Ca and Sr, the crystal structure becomes more compact as predicted by refined lattice parameters and density values (Table 1). Due to the compactness, the mobility is decreased as observed from Fig. 6, resulting in increased dc resistivity (Fig. 5). In BCFO sample, Ca does not replace Ba in proper quantity (as we have substituted) due to lower solubility of Ca as compared to iron and this is the reason that an additional phase (α-Fe_2O_3) appeared in the sample. This is also confirmed by Rietveld refinement of XRD results. Litsardakis et al. [24] have also reported the secondary phase (α-Fe_2O_3) along with the main phase due to lower solubility of substituted rare earth ions in M-type structure. On the other hand, Ba and Sr have higher solubility than Ca, therefore impurity phase is not observed in BFO and BCSFO samples. Thus the low value of DC electrical resistivity of BCFO sample in comparison to BCSFO is again supported by the presence of secondary (Fe_2O_3) phase.

3.6. Dielectric properties

It is observed from Fig. 7 that the dielectric constant decreases with increasing frequency for all the prepared hexaferrites. In the low frequency region, the dielectric dispersion is large and it becomes independent in the high frequency region. This is due to the fact that the dielectric material exhibits induced electric moment under the influence of external electric field. In the high frequency region, the polarization of induced moments or electron exchange between Fe^{2+} and Fe^{3+} ions could not synchronize with the frequency of applied electric field. So, the dielectric constant attains a constant value above certain high frequency [25].

The variations of $\tan\delta$ with frequency (Fig. 8) are qualitatively similar with the variation of ε' with frequency. This dielectric behavior of ferrites exists in non-homogeneous layered structure of ceramic materials, as explained by Maxwell–Wagner's bi-layered model [26,27]. According to this model, ferrite consists of perfectly conducting grains separated by insulating grain boundaries. Under the influence of an applied field, displacements of charge carriers take place. If the resistances of grain boundaries are large, the charge carriers align themselves at grain boundaries. Thus the space charge polarization is built up at grain boundary which is governed by the available free charges on grain boundaries. This leads to large dielectric constant. According to Koops [28], in the low frequency region, grain boundaries are effective and in the high frequency region, grains are effective. Thus low value of polarization builds up at higher frequency in the material which leads to decrease in the dielectric constant.

The temperature dependence of $\tan\delta$ for all the samples is shown in Fig. 9. It is observed that $\tan\delta$ increases with temperature because the electrical conductivity for semiconductor ferrites increases with temperature due to the increase in the number of charge carriers and their mobilities which are thermally activated. It was found that the dielectric constant behaves in opposite manner as that of dc electrical resistivity so that the mechanism of

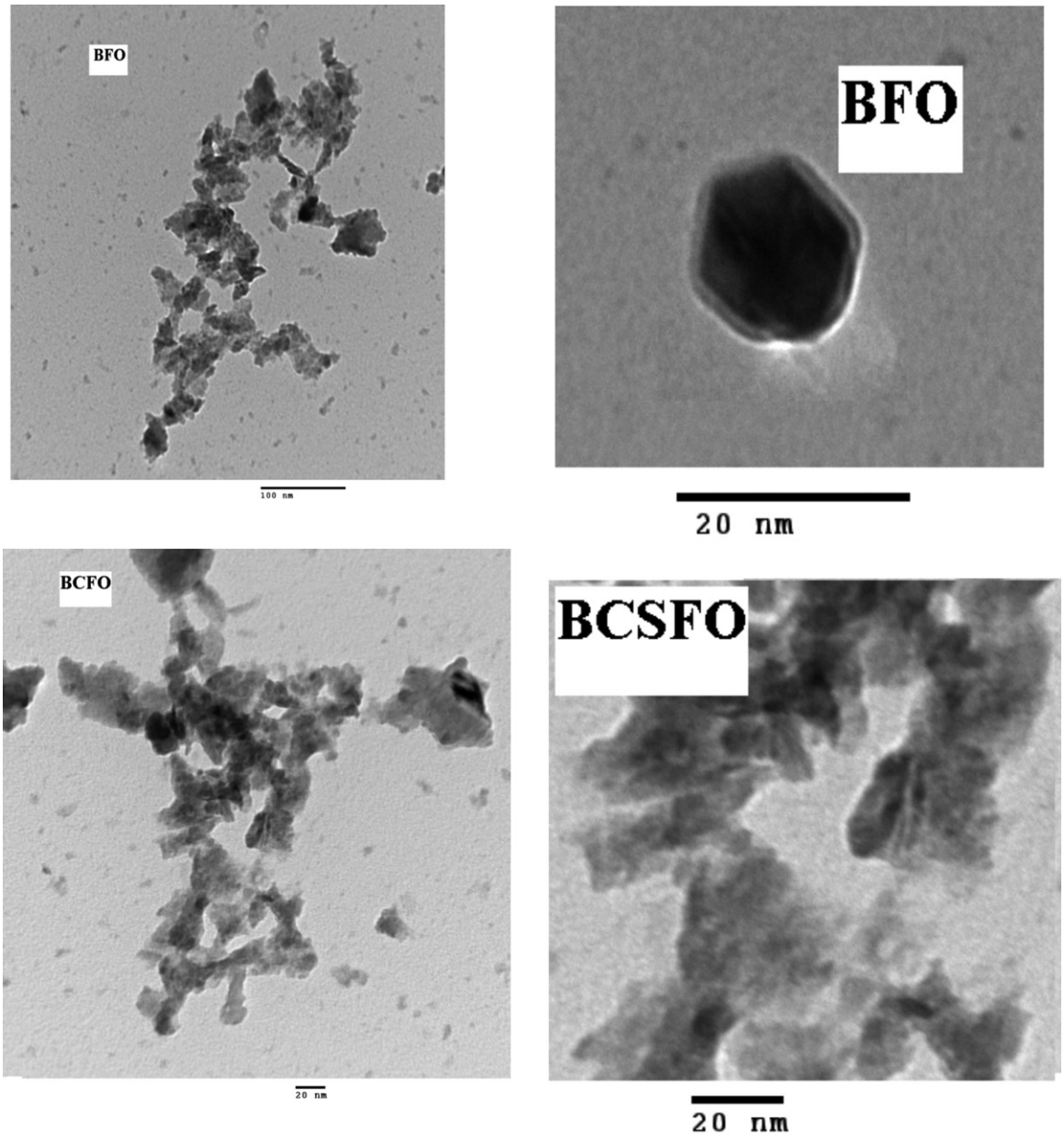

Fig. 4. TEM results of prepared hexaferrites.

Table 8
Magnetic parameters of prepared samples.

Sample	M_s (emu/g)	H_c (kOe)	M_r (emu/g)	M_r/M_s
BFO	53.04	2.75	25.47	0.48
BCFO	33.17	3.20	16.66	0.50
BCSFO	50.20	2.98	25.71	0.51

dielectric polarization is similar to that of electrical conduction which is a good proof of the Iwauchi's assumption [29].

3.7. Magnetic properties

Fig. 10 depicts the room temperature *M–H* hysteresis loops for all the prepared hexaferrites. The value of saturation magnetization (M_s) for BFO sample is about 53.04 emu/g at room temperature (Table 8), which is smaller than the theoretically predicted value 72 emu/g [30], but agrees well with other experimentally obtained values by different synthesis methods [31]. Several theories, including surface effect, spin canting and sample inhomogeneity have been proposed to account for the relatively low magnetization in fine particles [7]. According to ferromagnetic theory [32], coercivity H_c, for a uniaxial, single domain and non-interacting particle system is related to the magnetocrystalline anisotropy constant (κ) as:

$$H_c = \frac{\alpha\kappa}{\mu_0 M_S} \quad (6)$$

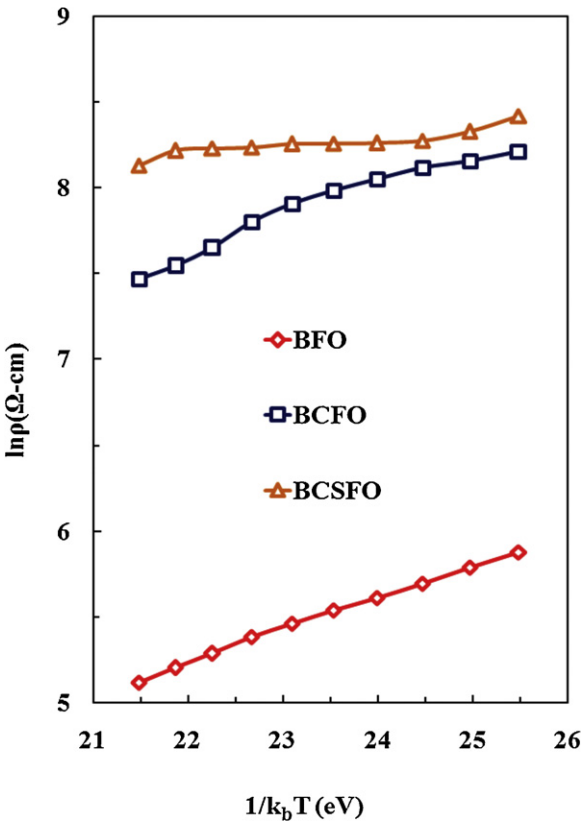

Fig. 5. Arrhenius plots of prepared hexaferrites.

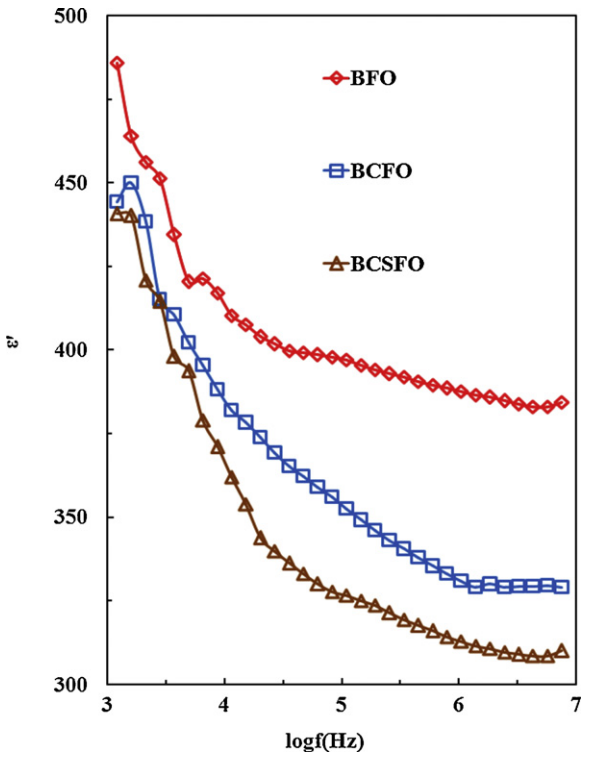

Fig. 7. Frequency dependence of dielectric constant (ε') of prepared samples at temperature 573 K.

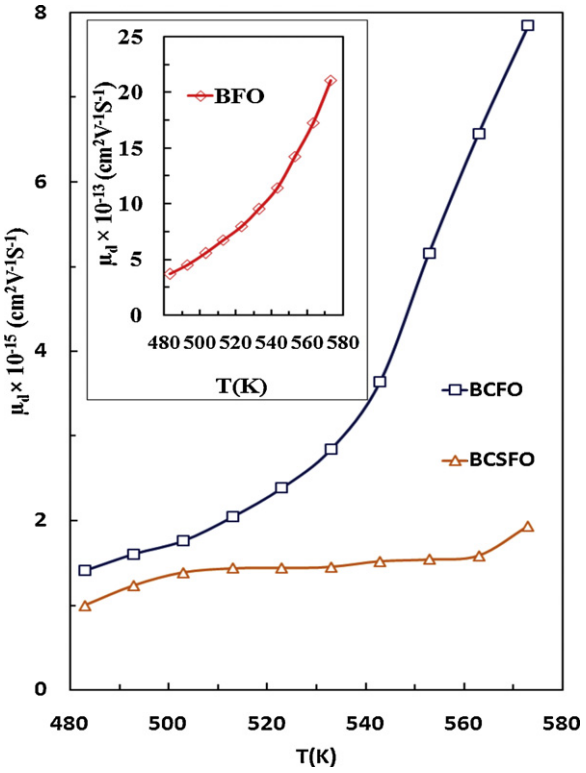

Fig. 6. Variation of drift mobility (μ_d) with temperature of all prepared hexaferrites.

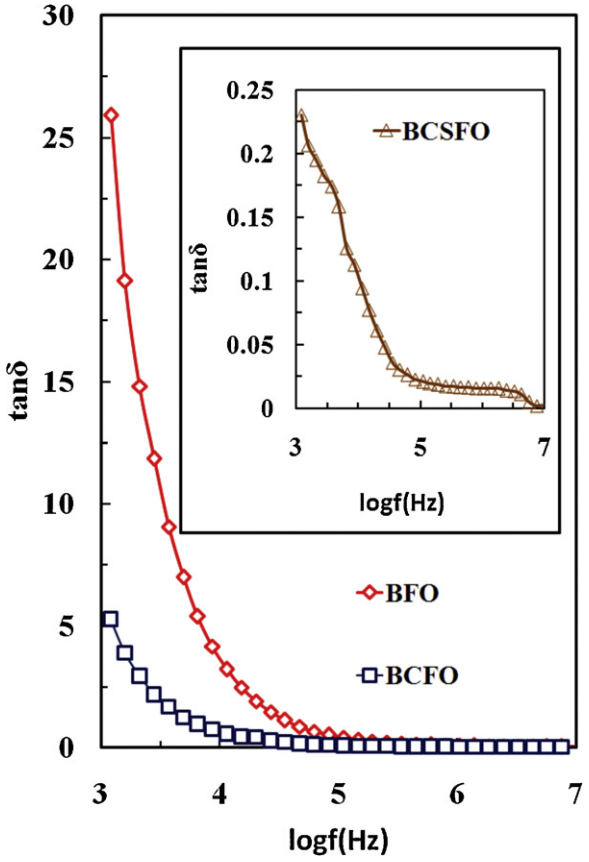

Fig. 8. Variation of dielectric loss ($\tan\delta$) of prepared samples with applied frequency at temperature 573 K.

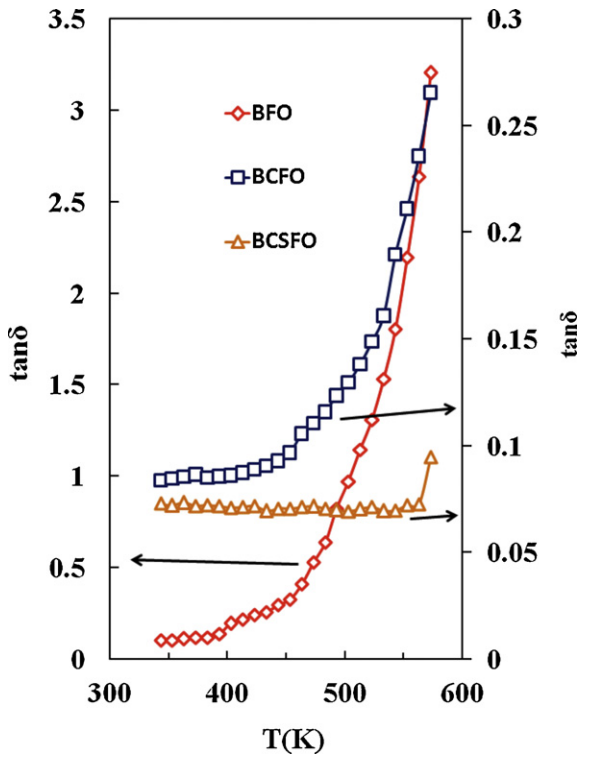

Fig. 9. Variation of dielectric loss ($\tan\delta$) of prepared samples with temperature at applied frequency 10 kHz.

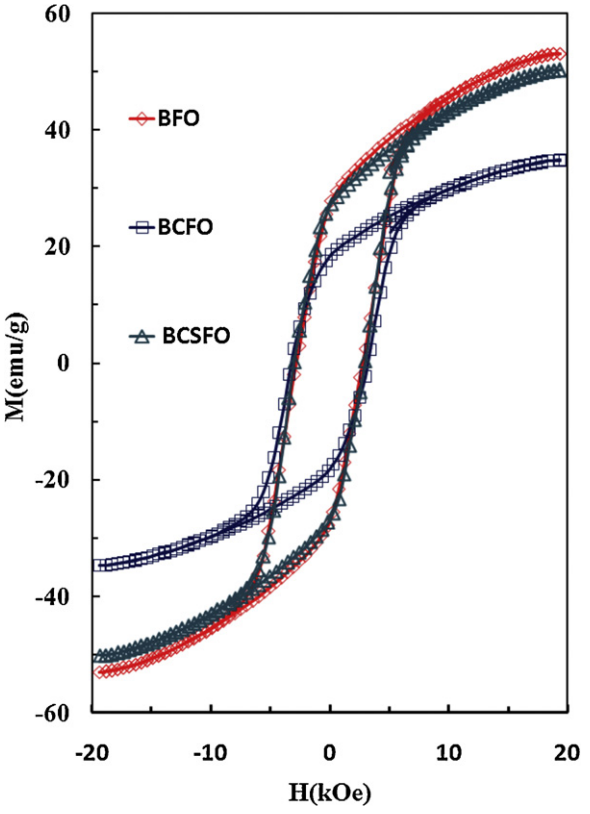

Fig. 10. Room-temperature *M–H* hysteresis loops of prepared samples.

where α is the orientation coefficient, which denotes the extent of coherent rotation for a non-interacting particle assembly and μ_0 is permittivity of the free space. In BCFO sample, low value of magnetization is due to presence of small amount of secondary phase (α-Fe_2O_3) which is a weak ferromagnetic. The resistance of particles increases during the domain rotation process due to non-magnetic α-Fe_2O_3 pinning. Hence value of M_s decreased from 53.04 emu/g to 33.17 emu/g. On contrary to it, coercivity (H_c) of both BCFO and BCSFO samples is increased to 3.20 kOe and 2.98 kOe, respectively, in comparison to BFO sample (2.75 kOe). It is due to the difference in the magnetocrystalline anisotropy of the Ca^{2+}, Sr^{2+} and Ba^{2+} ions. The increased magnetocrystalline anisotropy causes an enhancement in coercivity and the decrease in the value of M_s in BCSFO sample is according to Eq. (6). The Squareness ratio (SQR = M_r/M_s, where M_r is retentivity) is essentially a measure of squareness of the hysteresis loop. The SQR of all the samples is around 0.5 which is close to the expected value for randomly packed single domain particles if a coherent magnetization rotation reversal mechanism is assumed [33]. With substitution of Ca and Sr in BFO sample, the value of SQR increases up to 0.51 (Table 8). In general, large SQR value is preferred in many applications such as magnetic recording media of high density and permanent magnets [34].

4. Conclusions

$BaFe_{12}O_{19}$ (BFO), $Ba_{0.5}Ca_{0.5}Fe_{12}O_{19}$ (BCFO) and $Ba_{0.5}Ca_{0.25}Sr_{0.25}Fe_{12}O_{19}$ (BCSFO) samples were synthesized by commercial solid state reaction technique. The X-ray diffraction analysis of the samples revealed existence of single phase identified by JCPDS file number 00-043-0002. However, in BCFO sample an additional impurity phase (α-Fe_2O_3) was observed at 33.70° (2θ) which is identified by JCPDS file number 00-072-6227. The Rietveld refinement of XRD results confirmed the single hexagonal phase with space group $P6_3/mmc$ (194) in all the samples and the additional secondary phase with space group R3c in BCFO sample. SEM/TEM results present heterogeneously distribution of grain sizes. Substitution of Ca and Sr in BFO sample causes increase in resistivity. The dielectric constant (ε') and dielectric loss factor ($\tan\delta$) decrease with frequency and are in good agreement with the dc electrical resistivity data. Both ε' and $\tan\delta$ decrease with Ca and Sr substitutions in BFO sample. The low value of saturation magnetization in BCFO sample is due to the presence of secondary phase (α-Fe_2O_3) which is weak ferromagnetic in nature. On the other hand, coercivity (H_c) of the substituted hexaferrites is higher than BFO sample. The enhanced value of SQR for BCSFO sample makes its suitability as magnetic recording media of high density and permanent magnets.

Acknowledgment

Authors are thankful to DST, New Delhi (FIST Scheme) for providing XRD facilities.

References

[1] M.J. Iqbal, S. Farooq, Mater. Chem. Phys. 118 (2009) 308.
[2] F.M.M. Pereira, C.A.R. Junior, M.R.P. Santos, R.S.T.M. Sohn, F.N.A. Freire, J.M. Sasaki, J.A.C. de Paiva, A.S.B. Sombra, J. Mater. Sci. 19 (2008) 627.
[3] M.J. Iqbal, M.N. Ashiq, I.H. Gul, J. Magn. Magn. Mater. 322 (2010) 1720.
[4] M.N. Ashiq, M.J. Iqbal, I.H. Gul, J. Alloys Compd. 487 (2009) 341.
[5] Y. Liu, M.G.B. Drew, Y. Liu, J. Wang, M. Zhang, J. Magn. Magn. Mater. 322 (2010) 814.
[6] Y. Bai, J. Zhou, Z. Gui, L. Li, J. Magn. Magn. Mater. 246 (2002) 140.
[7] M. Radwan, M.M. Rashad, M.M. Hessien, J. Mater. Process. Technol. 181 (2007) 106.
[8] Z. Durmus, H. Sozeri, M.S. Toprak, A. Baykal, Nano-Micro Lett. 3 (2) (2011) 194.
[9] G. Benito, M.P. Morales, J. Requena, V. Raposo, M. Vazquez, J.S. Moya, J. Magn. Magn. Mater. 234 (2001) 65.

[10] H. Yanbing, S. Jian, S. Lina, T. Quan, L. Qin, J. Hongxiao, J. Dingfeng, B. Hong, G. Hongliang, W. Xinqing, J. Alloys Compd. 486 (2009) 348.
[11] S. Singhal, A.N. Garg, K. Chandra, J. Magn. Magn. Mater. 285 (2005) 193.
[12] H.J. Kown, J.Y. Shin, J.H. Oh, J. Appl. Phys. 75 (1994) 6109.
[13] P. Wartewig, M.K. Krause, P. Esquinazi, S. Rosler, R. Sonntag, J. Magn. Magn. Mater. 192 (1999) 83.
[14] Joint Committee on Powder Diffraction Standard (JCPDS), International Center for Diffraction Data (JCPDS 00-043-0002).
[15] R. Martinez-Garcia, E.R. Ruiz, E.E. Rams, Mater. Lett. 50 (2001) 183.
[16] M. Sivakumar, A. Gedanken, W. Zhong, Y.W. Du, D. Bhattacharya, Y. Yeshurun, I. Felner, J. Magn. Magn. Mater. 286 (2004) 95.
[17] A.C. Larson, R.B. Von Dreele, LANL Report LAUR 86, 2000.
[18] B.H. Toby, J. Appl. Crystallogr. 34 (2001) 210.
[19] C. Mu, N. Chen, X. Pan, X. Shen, X. Gu, Mater. Lett. 62 (2008) 840.
[20] Z. Durmus, B. Unal, M.S. Toprak, H. Sozeri, A. Baykal, Polyhedron 30 (2011) 1349.
[21] T. Abbas, M.U. Islam, M.A. Chaudhary, Mod. Phys. Lett. B 22 (1995) 1419.
[22] J. Smit, H.P.J. Wijn, Ferrites, Wiley, New York, 1959.
[23] E.J.W. Verwey, J.H. De Boer Ree, Trans. Chem. Des. Pays. Bas. 55 (1936) 531.
[24] G. Litsardakis, I. Manolakis, K. Efthimiadis, J. Alloys Compd. 427 (2007) 194.
[25] H.V. Keer, Principals of the Solid State, New Age Int. Pub. Ltd., Mumbai, 2000.
[26] J.C. Maxwell, Electricity and Magnetism, Vol. 1, Oxford University Press, Oxford, 1929 (Section 328).
[27] K.W. Wagner, Ann. Phys. 40 (1913) 817.
[28] C.G. Koops, Phys. Rev. 83 (1951) 121.
[29] K. Iwauchi, Jpn. J. Appl. Phys. 10 (1971) 1520.
[30] B.T. Shirk, W.R. Buessem, J. Appl. Phys. 40 (1969) 1294.
[31] H. Sozeri, J. Alloys Compd. 486 (2009) 809.
[32] R.J. Parker, Ferrite, Proceedings of ICF-3, 1980.
[33] E.C. Stoner, E.P. Wohlfarth, Philos. Trans. R. Soc. Lond. 240 (1948) 599.
[34] Z.F. Zi, Y.P. Sun, X.B. Zhu, Z.R. Yang, J.M. Dai, W.H. Song, J. Magn. Magn. Mater. 320 (2008) 2746.